Available online at www.sciencedirect.com
ScienceDirect
Chemical Geology 246 (2007) 55–64
CHEMICAL GEOLOGY INCLUDING ISOTOPE GEOSCIENCE
www.elsevier.com/locate/chemgeo

Platinum-group elements of the Meishan Permian–Triassic boundary section: Evidence for flood basaltic volcanism

Lin Xu [a,b,c], Yangting Lin [a,*], Wenjie Shen [a], Liang Qi [c], Liewen Xie [a], Ziyuan Ouyang [b]

[a] State Key Laboratory of Lithospheric Evolution, Institute of Geology and Geophysics, Chinese Academy of Sciences, P.O. Box 9825, Beijing 100029, China
[b] National Astronomical Observatories, Chinese Academy of Sciences, Beijing 100012, China
[c] Institute of Geochemistry, Chinese Academy of Sciences, Guiyang 550002, China

Received 21 February 2007; received in revised form 30 August 2007; accepted 31 August 2007

Editor: J. Fein

Abstract

Permian–Triassic boundary sections record the most severe mass extinction event in geological history. However, there is a long-standing controversy of whether bolide impact and/or basaltic flood volcanism triggered the mass extinction. Platinum-group elements (PGEs) are enriched in most extraterrestrial materials, but highly depleted in the terrestrial crust materials. We analyzed Ir, Ru, Rh, Pt and Pd in a set of samples from the global stratotype section and point (GSSP) of the Permian–Triassic boundary at Meishan, China, using isotope dilution inductively coupled plasma mass spectrometry (ID-ICP-MS) and nickel sulfide fire assay (NiS-FA) combined with Te coprecipitation. The samples have no Ir anomaly (5–53 pg/g), and their PGE patterns normalized to chondrites are highly fractionated with Ir/Pd ratios of 0.02–0.03 × CI, distinct from most extraterrestrial materials. In contrast, these patterns are closely parallel to those of the Siberian and probably Emeishan flood basalts, suggestive of possible sources of PGEs from the basalts. The abundances of PGEs increase in order of the pyrite lamina on the top of bed 24, bed 25 and bed 26, and then decrease to bed 28, probably indicative of a maximum eruption of the flood basalts during deposition of bed 26. The new data favor massive volcanism, rather than extraterrestrial impact, as a major cause of the Permian–Triassic boundary mass extinction.

Keywords: Mass extinction; Permian–Triassic boundary event; Platinum-group elements; Extraterrestrial impact; Basaltic volcanism

1. Introduction

Iridium is highly depleted in terrestrial crust materials relative to most extraterrestrial materials; hence it is commonly used as a critical geochemical marker for bolide impacts. Alvarez et al. (1980) first reported anomalous enrichment of Ir in the world-wide spread cm-thick layer of white clay in the Cretaceous–Tertiary (K/T) boundary sections and proposed that impact of a large Earth-crossing asteroid caused the extinction of dinosaurs. The Ir anomaly has been confirmed in many K/T boundary sections throughout the world (Alvarez et al., 1990), and the bolide impact hypothesis is supported by other lines of evidence, including carbon soot (Wolbach et al., 1988), Fullerenes (C60) with ^{3}He-enriched noble gases (Heymann et al., 1994), shocked quartz (Bostwick and Kyte, 1996), fragments of meteorites (Kyte, 1998; Bauluz et al., 2000), and the

* Corresponding author. Tel.: +86 10 62007112; fax: +86 10 62010846.
E-mail address: LinYT@mail.igcas.ac.cn (Y. Lin).

0009-2541/$ - see front matter © 2007 Elsevier B.V. All rights reserved.
doi:10.1016/j.chemgeo.2007.08.013

Chicxulub impact crater (Hildebrand and Boynton, 1990; Swisher et al., 1992; Morgan et al., 1997).

Permian–Triassic (P/Tr) boundary sections probably have recorded the most severe mass extinction event in the past 540 million years (Erwin, 1994; Jin et al., 2000; Benton et al., 2004). Abrupt ecosystem changes at the P/Tr boundary have been documented, such as marine anoxia (Wignall and Twitchett, 1996), increase of atmospheric CO_2 content (Berner, 2002), global warming (Huey and Ward, 2005), carbon isotopic excursions (Payne et al., 2004) and acid rains (Liang, 2002; Maruoka et al., 2003). However, the causes of these disturbances are enigmatic. Different from the Cretaceous–Tertiary boundary event, evidence for extraterrestrial impact of the P/Tr boundary is frail. Xu et al. (1985) reported ~2 ng/g of Ir in samples from the Meishan P/Tr boundary section, China, which was not confirmed in later studies (Clark et al., 1986; Zhou and Kyte, 1988). Fullerenes with extraterrestrial noble gases were first found in the same section (Becker et al., 2001) and later in the P/Tr boundary section at Graphite Peak, Antarctica (Poreda and Becker, 2003). However, Farley et al. (2001) analyzed samples of the Meishan section and found no extraterrestrial ^{3}He. Stronger evidence for a bolide impact is the discovery of chondritic fragments in the P/Tr boundary section in Antarctica (Basu et al., 2003).

Beside extraterrestrial impact, another widely accepted hypothesis for the end-Permian mass extinction is eruption of vast flood volcanism that could cause catastrophic changes of the ecosystem (Courtillot et al., 1999; Wignall, 2001; Grard et al., 2005). The P/Tr boundary event took place at about 251 Ma (Bowring et al., 1998; Mundil et al., 2004), contemporary with activity of the Siberian Traps (Campbell et al., 1992; Renne et al., 1995; Reichow et al., 2002; Kamo et al., 2003). Ages of the Emeishan large igneous province are controversial. The eruption of Emeishan basalts was reported to overlap temporally the P/Tr boundary event (Boven et al., 2002; Lo et al., 2002), or to predate the latter (Guo et al., 2004; Zhou et al., 2006; He et al., 2007). Zhou and Kyte (1988) showed that the clay layers of the P/Tr boundary sections were strongly enriched in Cs, Zr, Hf, Ta and Th and depleted in Cr, Co and Ir, and suggested that the clay was altered volcanic ash.

Previous analyses of Ir and other trace elements were usually carried out by radiochemical neutron activation analysis (RNAA) that is sensitive to Ir but not other platinum-group elements (PGEs) (e.g., Xu et al., 1985; Clark et al., 1986; Zhou and Kyte, 1988). In order to clarify the issue of Ir anomaly, we analyzed all PGEs (except for Os) of the P/Tr boundary section at Meishan, using isotope dilution inductively coupled plasma mass spectrometry (ID-ICP-MS) and nickel sulfide (NiS) fire assay combined with Te coprecipitation. The PGE patterns, instead of the abundances of Ir solely, have additional constraints on the sources of these elements. In addition, large masses of the samples (10–20 g) were analyzed in this study, hence the results are more representative for PGEs.

2. Samples and experiments

2.1. Samples

The P/Tr boundary section locates at Meishan, Changxing County, China (Fig. 1a). Exposed in this section is a series of quarries (Fig. 1b). The boundary between layers of bed 27b and 27c at Quarry D was defined as the Global Stratotype Section and Point (GSSP) of the P/Tr boundary according to the first appearance of *Hindeodus parvus* (Yin et al., 1996, 2001). However, the P/Tr catastrophic event (or geochemical) boundary lies about 10 cm below, recognized as the "boundary clay" of beds 25 and 26 or probably the pyrite lamina on the top of bed 24e (Bowring et al., 1998; Jin et al., 2000; Yin et al., 2001). The pyrite lamina is thin (~0.3 cm thick) and consists predominantly of pyrite. It is labeled as bed 24f hereafter. Bed 25 is composed of two layers of clay. The lower layer is light gray (0.5 cm thick) labeled as bed 25a, and the upper one is dark gray (2–3 cm thick) labeled as bed 25b. Bed 26 is composed of marl (8 cm thick), and it was divided artificially into two equal parts labeled as bed 26a (lower) and bed 26b (upper). Bed 27 consists of limestone (18 cm), which was subdivided into a, b, c and d upwards. Bed 28 is composed of white clay (3 cm thick). In order to study Ir and other PGEs of P/Tr boundary section, we collected a complete set of samples of the event boundary, including beds 24f, 25a, 25b, 26a and 26b from a fresh outcrop of Quarry C that locates about 400 m southwest to the GSSP and has recently been blasted. We also sampled the clay layer of bed 28, used as the background of PGEs because it postdated the mass extinction event. All samples were collected with plastic spades and packed in plastic bags. Rock of bed 27 was not analyzed in this study, because it deposited after the P/Tr catastrophic event and the limestone contains very low PGEs.

The pyrite lamina and clay samples were ground to <200 μm in an agate mortar, respectively. The mudstone samples of bed 26 were first broken into small fragments by freeze–thaw using liquid nitrogen, and then ground to <200 μm. To avoid contamination between samples, the agate mortar and pestle were washed 3 times with

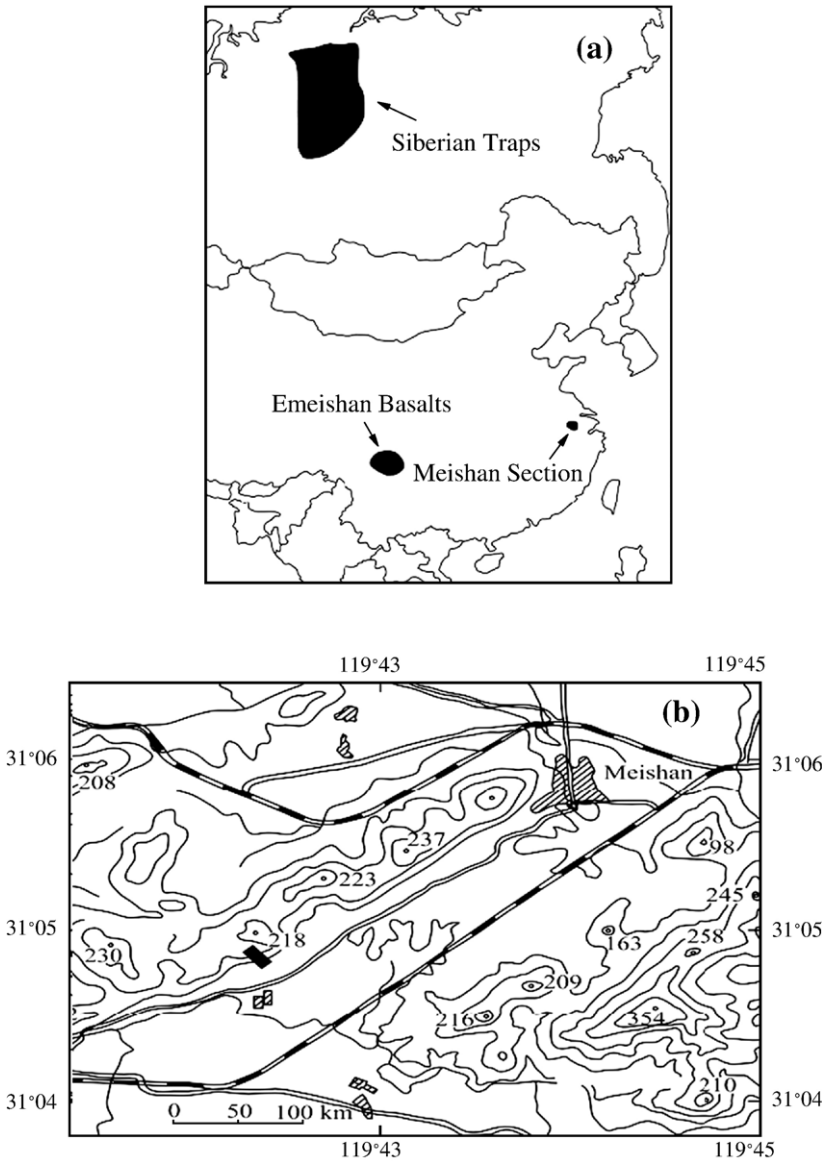

Fig. 1. (a) A sketch map showing locations of Meishan, the Siberial and Emeishan flood basalts. (b) A map showing the quarry region of the Meishan P/Tr boundary section. Locations of Quarry C, from where we sampled the rocks, and Quarry D, i.e. the GSSP, cannot be distinguished, marked as a black rectangle. The map is modified after Yin et al. (2001).

distilled water by ultrasonic cleaning, and then cleaned with ethanol and high-purity deionized water (18 MΩ/cm), respectively. About 50 g of each powder sample was dried overnight at 105 °C in an oven.

Another set of samples of fine-grained fractions (<25 μm) of bed 25 and 26 were also prepared for NiS fire assay analysis. They were separated from large masses of bed 25 (1.18 kg) and bed 26 (1.35 kg), and account for 98% of bed 25 and 95% of bed 26, respectively. The fine-grained samples were labeled as bed 25FG and bed 26FG, respectively. The other fractions with larger grain sizes were preserved for mineralogical study that was not reported here.

2.2. NiS fire assay method

20 g of each sample of bed 25a, bed 25b, bed 25FG and bed 26FG was analyzed using the NiS fire assay method. The reference material used in this study is WGB-1 gabbro. The details of the NiS fire assay method were described by Plessen and Erzinger (1998). In summary, 20 g of sample was fully mixed with 20 g of

Table 1
Blank level and determination limit of PGEs (ng/g)

Samples	Methods	Ir	Ru	Rh	Pt	Pd
Blank level	NiS fire assay	0.005	0.057	0.020	0.36	0.48
Determination limit (n=2, 10 σ)	NiS fire assay	0.009	0.076	0.019	0.13	0.18
Blank level	ID-ICP-MS	0.001	0.008	0.002	0.045	0.025
Determination limit (n=6, 10 σ)	ID-ICP-MS	0.004	0.050	0.016	0.23	0.13

di-lithium tetraborate, 10 g of sodium carbonate, 6.5 g of SiO_2, 2 g of nickel carbonyl, and 2 g of sublimated sulfur. The samples, reference material, and blank were melted in clay crucibles at 1150 °C for 2 h. The NiS buttons were then dissolved in 100 mL of 6 N HCl in 150 mL Savillex screw-capped Teflon beakers on a hot plate (90 °C) for 3 days. PGEs in the solutions were separated from the matrix through Te coprecipitation by adding 2 mL of 1 mg/mL Te and 4 mL of 1 M $SnCl_2$. The Te precipitates were dissolved in 2.5 mL of *aqua regia* (at 80 °C for 4 h) and then diluted to 25 mL with internal reference isotopes of ^{111}Cd and ^{185}Re (~10 ppb). All of the chemical procedures were carried out in an ultra-clean laboratory at the Institute of Geology and Geophysics, Chinese Academy of Sciences. The solutions were measured on a VG Plasma-Quad ExCell ICP-MS at the National Research Center for Geological Analysis, Chinese Academy of Geological Sciences.

All of the powder reagents used in this study were of guaranteed reagent grade. HCl and HNO_3 were purified by sub-boiling distillation. High-purity deionized water (18 MΩ/cm) was obtained from a Milli-Q system. The blank level and determination limit of the NiS fire assay method are listed in Table 1. The blank level is the average concentration of two procedural reagent blanks, and the determination limit was calculated to be 10 times the square root of average counts of the blanks divided by the sensitivity of 10 ng/mL PGE standard solution.

2.3. ID-ICP-MS method

10 g of each sample from the P/Tr boundary section was first heated in an oven at 700 °C for 1–2 h to incinerate any organic compounds and/or elemental carbon. The procedure for PGE separation and measurement follows the improved ID-ICP-MS method described by Qi et al. (2004). In general, 12 ng Pt, 10 ng Pd, 0.4 ng Ir and 0.7 ng Ru enriched isotope spikes were added to the samples. Silicates in the samples were dissolved with 45 mL of concentrated HF that was added in two times and each time the solution was evaporated to dryness on a hot plate. 15 mL of *aqua regia* were added to the residue and heated to 80 °C for 1 hour, and then slowly evaporated to dryness. The treatment with *aqua regia* was repeated once. Any remained HNO_3 was then driven out by adding 8 mL of concentrated HCl, and evaporated to dryness. Finally, the dried fraction was dissolved in 15 mL of concentrated HCl and 10 mL of water, and transferred into a 50 mL centrifuge tube. After centrifugation, the solution was transferred into a 150 mL glass beaker and 35 mL of 3% H_3BO_3 was added to the residue to dissolve fluorides. The process of dissolving fluorides with H_3BO_3 was repeated 3 times until the residue was <0.1 g, which was then transferred into a corundum crucible and evaporated to dryness. The last residue was fused with Na_2O_2, and then dissolved with water and HCl. This solution was added into the glass beaker.

The Te-coprecipitation step was the same as what is described above. The precipitate was then dissolved in 2 mL of *aqua regia*, and diluted to 10 mL. The solution was let to pass through the ion exchange column to eliminate interferences of Zr, Hf, Ni and Cu. The column consists of cation exchange resin of Dowex 50WX8 (200–400 mesh) and P507 extraction chromatograph resin (60–80 mesh). The elution was measured with the ICP-MS mentioned above. The concentrations of Ir, Ru, Pt and Pd were calculated by isotope dilution technique. Rh has only one isotope, hence it was calculated by using ^{194}Pt as the internal standard, because Pt and Rh have the same recoveries in the procedures (Qi et al., 2004).

Sub-boiling purified HF, HCl and HNO_3 were purchased from the Institute of Chemical Reagents, Beijing. The Ir and Rh contents of the acids were 0.2–0.4 pg/g, and the other PGEs were <8 pg/g. The $SnCl_2$ and Te solutions were purified by Te coprecipitation with each other. The H_3BO_3 solution was also purified by Te coprecipitation. All the Teflon and glass beakers were cleaned by boiling in fresh *aqua regia* before usage. The blank level and determination limit of the ID-ICP-MS method are given in Table 1. The blank level is average of six analyses of blanks that were prepared in the same way as the samples, and the determination limit is taken to be 10 times the standard deviation of the counts of the blanks divided by the sensitivity 10 ng/mL PGE standard solution. The blank level of ID-ICP-MS is approximately by a factor of 5–10 lower than the NiS fire assay mothed. The determination limit of the ID-ICP-MS is obviously higher than the blank level, but it is still clearly lower than the contents of PGEs in the

samples (Table 2). Analysis of Ru of the clay samples (i.e. beds 25, 26 and 28) has unknown interference to ^{99}Ru, hence the values are omitted from Table 2.

3. Results

3.1. NIS fire assay analysis

The PGE concentrations of the samples and reference material determined by the NiS fire assay method are summarized in Table 2. Our analysis of Rh for reference material, WGB-1, are in agreement with the certified value, while the abundances of other PGEs are slightly lower relative to the certified data. However, other literature data of WGB-1 are also systematically lower than the certified values, and are in good agreement with our analyses (Table 2).

The concentrations of PGEs in beds 25 and 26 are rather low, with the highest Ir of 0.053 ng/g in bed 26FG, suggestive of no positive Ir anomaly (Table 2). Furthermore, it is noticed that PGEs in bed 26FG are highly fractionated, with the Ir/Pd ratio of 0.05 × CI. The dark-colored clay of bed 25b contains higher PGEs in comparison with the light-colored clay of bed 25a that has nearly no PGEs detectible for the NiS fire assay method. This is consistent with the analysis of bed 25FG that is a mixture sample of bed 25a and bed 25b with the abundances of PGEs within the ranges of the latter, except for a slightly higher abundance of Pt in bed 25FG than bed 25b. In addition, PGEs in bed 25b are also strongly fractionated, with the Ir/Pd ratio of 0.02 × CI.

3.2. ID-ICP-MS analysis

The ID-ICP-MS analysis of the reference material WGB-1 is listed in Table 2. Although lower than the certified values, the result of ID-ICP-MS analysis is consistent with other literature data and that of NiS fire assay analysis (except for Rh). The discrepancy of Rh is probably attributable to the analytical methods. The analysis of Rh by the NiS fire assay method is similar to the certified value, while that by ID-ICP-MS agrees with the other literature data.

The ID-ICP-MS analyses of the P/Tr boundary samples reveal no positive Ir anomaly, with a range of 0.005–0.028 ng/g (Table 2). The abundance of Ir appears to increase from bed 25a to bed 25b, and then to a maximum at beds 26a and b (Fig. 2). The variation trend is consistent with the result of NiS fire assay analysis as mentioned above, although the value of bed 26FG by NiS fire assay is significantly higher than those of beds 26a and 26b by ID-ICP-MS. The pyrite lamina (bed 24f) is commonly referred to as the P/Tr event boundary, but it contains very low Ir (0.008 ± 0.003 ng/g). In contrast, the Ir content of bed 28 (0.015 ± 0.003 ng/g), which postdated the mass extinction, is higher than those of beds 24f and 25.

The other PGEs are correlated with Ir (Table 2). Fig. 2 also shows the Pd concentration profile of the Meishan P/Tr boundary section, which is parallel to that of Ir. Fig. 3 plots the CI-normalized abundances of PGEs of the samples, indicative of the highly fractionated patterns with the relative abundances increasing from

Table 2
Concentrations of PGEs in the Meishan P/Tr boundary section (ng/g)

	Number	Thickness (cm)	Ir	Ru	Rh	Pt	Pd	Note
Bed 28	6	3	0.015±0.003		0.045±0.020	0.375±0.036	0.873±0.314	ID-ICP-MS
Bed 26b	3	4	0.028±0.005		0.066±0.009	1.30±0.052	1.80±0.049	ID-ICP-MS
Bed 26a	3	4	0.027±0.003	0.085±0.030	0.052±0.026	1.03±0.046	1.38±0.083	ID-ICP-MS
Bed 25b	3	2–3	0.013±0.002		0.054±0.034	0.577±0.043	0.772±0.191	ID-ICP-MS
Bed 25a	3	0.5	0.005±0.001		0.038±0.009	0.256±0.067	0.359±0.165	ID-ICP-MS
Bed 24f	6	0.2–0.4	0.008±0.003	0.031±0.024	0.053±0.024	0.372±0.028	0.274±0.065	ID-ICP-MS
Bed 26FG	1	8	0.053	n.d.	0.063	1.21	1.15	NiS fire assay
Bed 25FG	1	2.5–3.5	n.d.	n.d.	n.d.	0.61	0.50	NiS fire assay
Bed 25b	1	2–3	0.011	n.d.	0.031	0.49	0.68	NiS fire assay
Bed 25a	1	0.5	n.d.	n.d.	n.d.	0.14	n.d.	NiS fire assay
WGB-1	5		0.153±0.026	0.144±0.079	0.167±0.011	5.25±0.95	11.5±1.4	ID-ICP-MS
	1		0.204	0.215	0.326	5.04	12.6	NiS fire assay
			0.33	*0.30*	*0.32*	*6.10*	*13.9*	*certified*
			0.23±0.02	*0.16±0.04*	*0.19±0.02*	*5.74±0.65*	*12.0±1.7*	*Qi*
			0.27	*0.16*		*4.71*	*11.7*	*Meisel*
			0.20±0.04	*0.20±0.04*	*0.14±0.01*	*3.8±1.0*	*13.0±1.1*	*Plessen*
			0.20±0.02	*0.17±0.03*	*0.15±0.01*	*4.20±0.50*	*12.90±0.5*	*Jin*

Note: n.d. = below the determination limit. The analytical results are given as mean ± σ. Literature data (italic) after Qi et al. (2004), Meisel et al., (2001), Plessen and Erzinger (1998), and Jin and Zhu (2000).

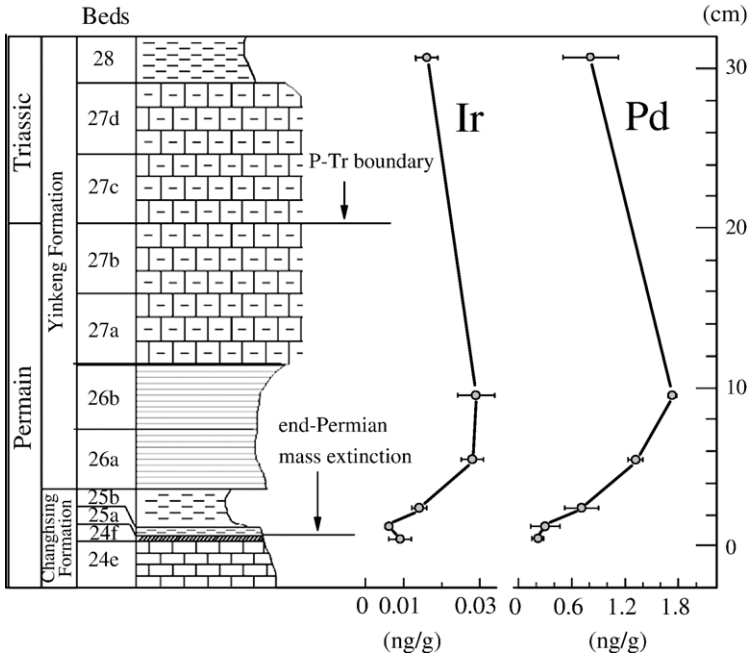

Fig. 2. Ir and Pd concentration profiles of the Meishan P/Tr boundary section, showing small peaks at bed 26. Bed 28 contains slightly higher Ir and Pd in comparison with beds 24f and 25, although the former postdated the P/Tr boundary event. The assignments of the beds after Yin et al. (2001).

left to right (in order of increasing volatility). The PGE patterns of individual samples are nearly parallel to each other, except for slight depletion of Pt in beds 24f, 25a and 28 relative to Rh. In addition, the ID-ICP-MS analyses are consistent with the results obtained by the NiS fire assay method (Table 2).

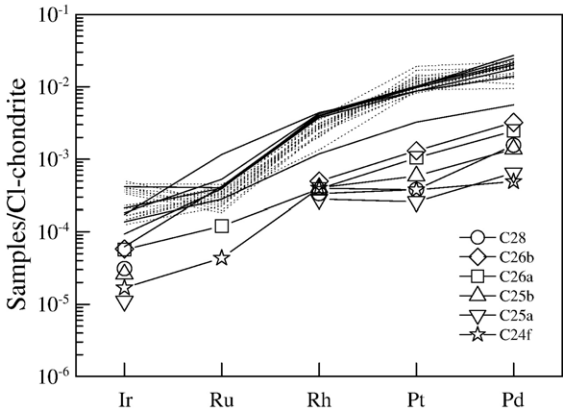

Fig. 3. The CI-normalized PGE patterns of the Meishan P/Tr boundary section are highly fractionated, with the relative abundances increasing from left to right (in order of increasing volatility). These patterns are nearly parallel to each other, except for slight depletions of Pt in beds 24f, 25 and 28. The Siberian basalts (solid lines) (Lightfoot and Keays, 2005) and Emeishan basalts (dotted lines) (Song et al., 2006) are shown for comparison, which are also parallel to the P/Tr boundary samples, especially to bed 26. Data of CI chondrite are from Anders and Grevesse (1989).

4. Discussion

4.1. Evidence against extraterrestrial impact

The presence of an iridium anomaly in event boundary sections is one of the crucial arguments for extraterrestrial impacts responsible for mass extinction. A well-studied example is the Ir anomaly of the K/T boundary sections (Alvarez et al., 1980). However, the Ir anomaly of the P/Tr boundary sections is disputed. Xu et al. (1985) analyzed Ir of the Meishan P/Tr boundary section using RNAA, and reported an Ir concentration of 2 ng/g. In contrast, Zhou and Kyte (1988) found very low Ir concentrations (0.003–0.087 ng/g) in the same section using RNAA. Our data of the Meishan section revealed no positive Ir anomaly either (Table 2), strongly confirming Zhou and Kyte's results.

The absence of Ir anomaly could not be due to heterogeneous distribution of PGEs in the samples. In comparison with small masses (80–120 mg) of samples for RNAA, much larger samples were used for NiS fire assay (about 20 g) and ID-ICP-MS (about 10 g) analyses, hence the results of the latter are more representative. Moreover, the fine-grained fractions of beds 25 and 26 were prepared from more than 1 kg of samples from each bed, and they were thoroughly mixed during the size separating procedures. The analyses of beds 25FG and 26FG confirm no Ir anomaly in beds 25 and 26.

The pyrite lamina on the top of bed 24e could be the P/Tr event boundary, because that it is the onset layer of large negative excursions of $\delta^{13}C$ (Jin et al., 2000), $\delta^{34}S$ and $\delta^{87}Sr$ (Kaiho et al., 2001), and oceanic anoxia (Shen et al., 2007). Fullerenes and the captured ^{3}He-enriched noble gases were also reported in samples at the base of bed 25 of the Meishan section (Becker et al., 2001). However, the pyrite lamina (bed 24f) and the lower part of bed 25 (bed 25a) contain the lowest Ir (0.008± 0.003 ng/g, 0.005±0.001 ng/g) and other PGEs (Table 2). The deposition of bed 28 postdated the mass extinction, and it contains even higher Ir and other PGEs than beds 24f and 25a. If a bolide impact were the main cause of the P/Tr boundary event, higher abundances of Ir and other PGEs would have been found in beds 24f and/or 25a than in the other beds.

Another key line of evidence against extraterrestrial impact is the highly fractionated patterns of PGEs in the Meishan P/Tr boundary section (Fig. 3). Most of meteorites (>96% in number) are undifferentiated (namely chondrites), hence have flat PGE patterns normalized to CI chondrites, obviously distinct from the strongly Ir-depleted patterns of the Meishan P/Tr boundary section. Chondritic meteorite fragments were found at the P/Tr boundary in Antarctica (Basu et al., 2003), taken as evidence for the bolide impact hypothesis. However, this is inconsistent with the fractionated PGE patterns. Furthermore, as mentioned above, the PGE patterns of beds 24f, 25 and 26 are nearly parallel to that of bed 28 deposited after the mass extinction event, suggestive of their similar terrestrial sources.

Fig. 4 plots elemental ratios with Ir/Pt vs. Pd/Pt. It is clear that the Meishan boundary samples are far from the chondritic meteorites, arguing against for a genetic link between them. In contrast, the K/T boundary samples overlap with chondritic materials.

It is unlikely that the highly fractionated PGE patterns and elemental ratios of the samples were modified from a flat pattern of chondritic materials by postdeposition processes, such as biological activity. The different colors of the clay layers of beds 25, 26 and 28 suggest various degrees of biological activity, and the pyrite lamina is composed predominantly of pyrite. However, all of the samples have nearly parallel PGE patterns, suggestive of a similar source and no significant secondary effects. In fact, the PGEs patterns of the samples are parallel to those of the Siberian (and probably Emeishan) basalts (see next subsection), and this could not be coincident.

Assuming terrestrial origins of the PGEs in the P/Tr boundary samples, the highest abundance of Ir of bed 26 (0.028 ng/g) can be referred to as the background, hence it is used to estimate the detection limit of chondritic materials in the boundary samples. Taking the Ir content of CI chondrites (480 ng/g) for the possible projectile and that of bed 26 (0.028 ng/g) as the background, the detection limit can be estimated to be as low as 6×10^{-5} based on mass balance. This means that presence of chondritic materials with abundance of less than 60 ppm in the boundary samples cannot be detected.

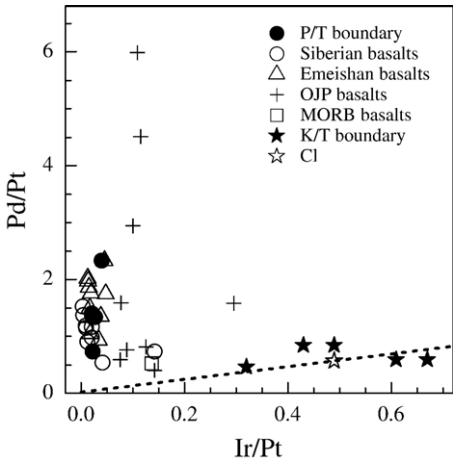

Fig. 4. Ir/Pt vs. Pd/Pt plots of the Meishan P/Tr boundary section. Our analyses of the Meishan samples overlap with the majority of the Siberian basalts (Lightfoot and Keays, 2005) and Emeishan basalts (Song et al., 2006), except for a higher Ir/Pt ratio of the Gd unit that located at the bottom of the Siberian trap. The mid-ocean ridge basalts (MORB) and Ontong Java Plateau (OJP) basalts (Ely and Neal, 2003) have distinguishable ratios. It is evident that the Meishan samples plot far from literature values of the K–T boundary section (Kyte et al., 1985; Lee et al., 2003) that are consistent with CI chondrites. The dashed line shows chondritic ratio of Pd/Ir as a reference.

4.2. Evidence for volcanic eruption

Besides bolide impact, the P/Tr boundary event may be related to vast eruption of flood basalts (Wignall, 2001; Grard et al., 2005). Zircon U–Pb ages of the P/Tr boundary ashes (250.0–251.4 Ma) (Renne et al., 1995; Bowring et al., 1998) are synchronous with the eruption of Siberian flood basalts (249.4–250 Ma) (Renne et al., 1995; Reichow et al., 2002) (Kamo et al., 2003). Our analyses of the Meishan samples provide with crucial evidence for a similar reservoir of PGEs in the P/Tr boundary samples and Siberian flood basalts. In Fig. 3, it is noted that the PGE patterns of the Meishan samples are closely parallel to majority of the Siberian basalts. Furthermore, elemental ratios PGEs of the P/Tr boundary samples also overlap with the latter, but are distinguished from the mid-ocean ridge basalts (MORB) and Ontong Java Plateau (OJP) basalts (Fig. 4).

The Emeishan flood basalts are widespread in southwestern China and northern Vietnam (Fig. 1a). Although many zircon U–Pb ages of the Emeishan basalts are ~260 Ma (Zhou et al., 2006; He et al., 2007), ^{39}Ar–^{40}Ar ages of ~251–253 Ma were also reported (Lo et al., 2002), which are consistent with the newly obtained U–Pb dates of the P/Tr boundary event (252.6±0.2 Ma) (Mundil et al., 2004). Our analyses of the Meishan samples show rather similar elemental patterns and ratios of PGEs in comparison with the Emeishan basalts, except for slight positive Pt anomalies and negative Ru anomalies in the majority of the latter (Figs. 3 and 4). We cannot exclude the Emeishan basalts as a possible resource of PGEs in the Meishan P/Tr boundary section.

The concentrations of PGEs in the Meishan P/Tr boundary section can be used as an indicator for the intensity of flood basalt volcanism. As shown in Fig. 2, the concentrations of Ir and Pd increase from the pyrite lamina to bed 26 and then decrease to bed 28, indicative of a maximum eruption of basalt volcanism during the deposition of bed 26. This main eruption event probably triggered the mass extinction recorded in the P/Tr boundary section. Although the black color of bed 26 probably indicates the presence of organic matter, its higher abundance of PGEs than other beds could not be a result of biological activity, because it has similar PGE patterns as the pyrite lamina and the other clay layers with different colors as discussed above.

Assuming all PGEs were contributed by the Siberian basalts, the contents of basaltic ashes in individual beds can be estimated according to the PGE abundances of the samples. Taking the average abundance of Pd (9.4 ng/g) of the Siberian basalts (Lightfoot and Keays, 2005) and that of bed 26b (1.8 ng/g), a maximum content of the basaltic ashes in the Meishan P/Tr boundary samples is about 20%. This implies that most of the boundary clay is composed of other highly PGE-depleted volcanic ashes, in consistency with previous work that the ashes are silicic volcanic origin according to enrichments in incompatible elements (e.g. Cs, Zr, Hf, Ta and Th) (Zhou and Kyte, 1988).

5. Conclusions

The Ir, Ru, Rh, Pt and Pd in the Meishan P/Tr boundary section were analyzed with both ID-ICP-MS and NiS fire assay in combination with Te coprecipitation, and the results obtained by both methods showed no Ir anomaly. Furthermore, the PGE patterns of the samples are highly fractionated relative to chondritic materials, arguing against extraterrestrial impact for mass extinction at the P/Tr boundary. However, achondrite-like projectiles highly depleted in siderophile elements cannot be excluded based on the lack of PGE anomaly.

On the other hand, our newly obtained data revealed the parallel PGE patterns of beds 24f, 25, 26 and 28, suggestive of origin from similar terrestrial sources as bed 28 postdated the mass extinction event. The PGE patterns are also similar to those of the Siberian and probably Emeishan basalts, providing evidence for a close relationship between the P/Tr boundary event and the eruption of flood basalts. The concentrations of PGEs increase from the pyrite lamina to bed 26 and then decrease to bed 28, indicating a maximum eruption of food basalts when bed 26 deposited. The main eruption event was probably related to the mass extinction event at the P/Tr boundary.

Acknowledgements

We thank Prof. Y. Jin and Dr. H. Zhang for providing us with information about the Meishan P/Tr boundary section, and Dr. W. Qu for assistance in ICP-MS analysis. The constructive reviews by two anonymous reviewers and the Editor J. Fein have significantly improved the manuscript. This study was supported by the One-Hundred-Talent Program and the Pilot Project of Knowledge Innovation Program (Grant No. kzcx2-yw-110) of the Chinese Academy of Sciences, and by the National Natural Science Foundation of China (Grant No. 40232026).

References

Alvarez, L.W., Alvarez, W., Asaro, F., Michel, H.V., 1980. Extraterrestrial cause for the Cretaceous–Tertinary extinction. Science 208, 1095–1108.

Alvarez, W., Asaro, F., Montanari, A., 1990. Iridium profile for 10 million years across the Cretaceous–Tertiary boundary at Gubbio (Italy). Science 250, 1700–1702.

Anders, E., Grevesse, N., 1989. Abundances of the elements: meteoritic and solar. Geochim. Cosmochim. Acta 53, 197–214.

Basu, A.R., Petaev, M.I., Poreda, R.J., Jacobsen, S.B., Becker, L., 2003. Chondritic meteorite fragments associated with the Permian–Triassic boundary in Antarctica. Science 302, 1388–1392.

Bauluz, B., Peacor, D.R., Elliott, W.C., 2000. Coexisting altered glass and Fe–Ni oxides at the Cretaceous–Tertiary boundary, Stevns Klint (Denmark): direct evidence of meteorite impact. Earth Planet. Sci. Lett. 182, 127–136.

Becker, L., Poreda, R.J., Hunt, A.G., Bunch, T.E., Rampino, M., 2001. Impact event at the Permian–Triassic boundary: evidence from extraterrestrial noble gases in fullerenes. Science 291, 1530–1533.

Benton, M.J., Tverdokhlebov, V.P., Surkov, M.V., 2004. Ecosystem remodeling among vertebrates at the Permian–Triassic boundary in Russia. Nature 432, 97–100.

Berner, R.A., 2002. Examination of hypotheses for the Permo-Triassic boundary extinction by carbon cycle modeling. Proc. Natl. Acad. Sci. 99, 4172–4177.

Bostwick, J.A., Kyte, F.T., 1996. The size and abundance of shocked quartz in Cretaceous–Tertiary boundary sediments from the Pacific basin. Geol. Soc. Am. Spec. Pap. 307, 403–415.

Boven, A., Pasteels, P., Punzalan, L.E., Liu, J., Luo, X., Zhang, W., Guo, Z., Hertogen, J., 2002. 40Ar/39Ar geochronological constraints on the age and evolution of the Permo-Triassic Emeishan Volcanic Province, Southwest China. J. Asian Earth Sci. 20, 157–175.

Bowring, S.A., Erwin, D.H., Jin, Y.G., Martin, M.W., Davidek, K., Wang, W., 1998. U/Pb zircon geochronology and tempo of the End-Permian mass extinction. Science 280, 1039–1045.

Campbell, I.H., Czamanske, G.K., Fedorenko, V.A., Hill, R.I., Stepanov, V., 1992. Synchronism of the Siberian Traps and the Permian–Triassic boundary. Science 258, 1760–1763.

Clark, D.L., Wang, C., Orth, C.J., Gilmore, J.S., 1986. Conodont survival and low iridium abundance across the Permian–Triassic boundary in South China. Science 233, 984–986.

Courtillot, V., Jaupart, C., Manighetti, I., Tapponnier, P., Besse, J., 1999. On causal links between flood basalts and continental breakup. Earth Planet. Sci. Lett. 166, 177–195.

Ely, J.C., Neal, C.R., 2003. Using platinum-group elements to investigate the origin of the Ontong Java Plateau, SW Pacific. Chem. Geol. 196, 235–257.

Erwin, D.H., 1994. The Permo-Triassic extinction. Nature 367, 231–236.

Farley, K.A., Mukhopadhyay, S., Isozaki, Y., Becker, L., Poreda, R.J., 2001. An extraterrestrial impact at the Permian–Triassic boundary? Science, 293, p. 2343a.

Grard, A., Francois, L.M., Dessert, C., Dupre, B., Godderis, Y., 2005. Basaltic volcanism and mass extinction at the Permo-Triassic boundary: environmental impact and modeling of the global carbon cycle. Earth Planet. Sci. Lett. 234, 207–221.

Guo, F., Fan, W., Wang, Y., Li, C., 2004. When did the Emeishan mantle plume activity start? Geochronological and geochemical evidence from ultramafic–mafic dikes in Southwestern China. Int. Geol. Rev. 46, 226–234.

He, B., Xu, Y.-G., Huang, X.-L., Luo, Z.-Y., Shi, Y.-R., Yang, Q.-J., Yu, S.-Y., 2007. Age and duration of the Emeishan flood volcanism, SW China: Geochemistry and SHRIMP zircon U–Pb dating of silicic ignimbrites, post-volcanic Xuanwei Formation and clay tuff at the Chaotian section. Earth Planet. Sci. Lett. 255, 306–323.

Heymann, D., Chibante, L.P.F., Brooks, R.R., Wolbach, W.S., Smalley, R.E., 1994. Fullerenes in the Cretaceous–Tertiary boundary layer. Science 265, 645–647.

Hildebrand, A.R., Boynton, W.V., 1990. Proximal Cretaceous–Tertiary boundary impact deposits in the Caribbean. Science 248, 843–847.

Huey, R.B., Ward, P.D., 2005. Hypoxia, global warming, and terrestrial late Permian extinctions. Science 308, 398–401.

Jin, X., Zhu, H., 2000. Determination of platinum group elements and gold in geological samples with ICP-MS using a sodium peroxide fusion and tellurium co-precipitation. J. Anal. At. Spectrom. 15, 747–751.

Jin, Y.G., Wang, Y., Wang, W., Shang, Q.H., Cao, C.Q., Erwin, D.H., 2000. Pattern of marine mass extinction near the Permian–Triassic boundary in south China. Science 289, 432–436.

Kaiho, K., Kajiwara, Y., Nakano, T., Miura, Y., Kawahata, H., Tazaki, K., Ueshima, M., Chen, Z., Shi, G.R., 2001. End-Permian catastrophe by a bolide impact: evidence of a gigantic release of sulfur from the mantle. Geology 29, 815–818.

Kamo, S.L., Czamanske, G.K., Amelin, Y., Fedorenko, V.A., Davis, D.W., Trofimov, V.R., 2003. Rapid eruption of Siberian flood-volcanic rocks and evidence for coincidence with the Permian–Triassic boundary and mass extinction at 251 Ma. Earth Planet. Sci. Lett. 214, 75–91.

Kyte, F.T., 1998. A meteorite from the Cretaceous/Tertiary boundary. Nature 396, 237–239.

Kyte, F.T., Smit, J., Wasson, J.T., 1985. Siderophile interelement variations in the Cretaceous–Tertiary boundary sediments from Caravaca, Spain. Earth Planet. Sci. Lett. 73, 183–195.

Lee, C.-T.A., Wasserburg, G.J., Kyte, F.T., 2003. Platinum-group elements (PGE) and rhenium in marine sediments across the Cretaceous–Tertiary boundary: constraints on Re-PGE transport in the marine environment. Geochim. Cosmochim. Acta 67, 655–670.

Liang, H., 2002. End-Permian catastrophic event of marine acidification by hydrated sulfuric acid: mineralogical evidence from Meishan section of south China. Chin. Sci. Bull. 47, 1393–1397.

Lightfoot, P.C., Keays, R.R., 2005. Siderophile and chalcophile metal variations in flood basalts from the Siberian trap, Noril'sk region: implications for the origin of the Ni–Cu–PGE sulfide ores. Econ. Geol. 100, 439–462.

Lo, C.-H., Chung, S.-L., Lee, T.-Y., Wu, G., 2002. Age of the Emeishan flood magmatism and relations to Permian–Triassic boundary events. Earth Planet. Sci. Lett. 198, 449–458.

Maruoka, T., Koeberl, C., Hancox, P.J., Reimold, W.U., 2003. Sulfur geochemistry across a terrestrial Permian–Triassic boundary section in the Karoo Basin, South Africa. Earth Planet. Sci. Lett. 206, 101–117.

Meisel, T., Moser, J., Fellner, N., Wegscheider, W., Schoenberg, R., 2001. Simplified method for the determination of Ru, Pd, Re, Os, Ir and Pt in chromitites and other geological materials by isotope dilution ICP-MS and acid digestion. Analyst 126, 322–328.

Morgan, J., Warner, M., and the Chicxulub Working Group, 1997. Size and morphology of the Chicxulub impact crater. In: Brittan, J., Buffler, R., Camargo, A., Christeson, G., Denton, P., Hildebrand, A., Hobbs, R., Macintyre, H., MacKenzie, G., Maguire, P., Marin, L., Nakamura, Y., Pilkington, M., Sharpton, V., Snyder, D., Suarez, G., Trejo, A. (Eds.), Nature, 390, pp. 472–476.

Mundil, R., Ludwig, K.R., Metcalfe, I., Renne, P.R., 2004. Age and timing of the Permian mass extinctions: U/Pb dating of closed-system zircons. Science 305, 1760–1763.

Payne, J.L., Lehrmann, D.J., Wei, J., Orchard, M.J., Schrag, D.P., Knoll, A.H., 2004. Large perturbations of the carbon cycle during recovery from the end-Permian extinction. Science 305, 506–509.

Plessen, H.G., Erzinger, J., 1998. Determination of the platinum-group elements and gold in twenty rock reference materials by inductively coupled plasma-mass spectrometry (ICP-MS) after pre-concentration by nickel sulfide fire assay. Geostan. Newsl. 22, 187–194.

Poreda, R.J., Becker, L., 2003. Fullerenes and interplanetary dust at the Permian–Triassic boundary. Astrobiology 3, 75–90.

Qi, L., Zhou, M., Wang, C.Y., 2004. Determination of low concentrations of platinum group elements in geological samples by ID-ICP-MS. J. Anal. At. Spectrom. 19, 1335–1339.

Reichow, M.K., Saunders, A.D., White, R.V., Pringle, M.S., Al'Mukhamedov, A.I., Medvedev, A.I., Kirda, N.P., 2002. $^{40}Ar/^{39}Ar$ dates from the west Siberian basin: Siberian flood basalt province doubled. Science 296, 1846–1849.

Renne, P.R., Black, M.T., Zhang, Z., Richards, M.A., Basu, A.R., 1995. Synchrony and causal relations between Permian–Triassic boundary crises and Siberian flood volcanism. Science 269, 1413–1416.

Shen, W., Lin, Y., Xu, L., Li, J., Wu, Y., Sun, Y., 2007. Pyrite framboids in the Permian–Triassic boundary section at Meishan, China: Evidence for dysoxic deposition. Palaeogeogr. Palaeoclimatol. Palaeoecol. 253, 323–331.

Song, X.Y., Zhou, M.F., Keays, R.R., Cao, Z.M., Sun, M., Qi, L., 2006. Geochemistry of the Emeishan flood basalts at Yangliuping, Sichuan, SW China: implications for sulfide segregation. Contrib. Mineral. Petrol. 152, 53–74.

Swisher III, C.C., Grajales-Nishimura, J.M., Montanari, A., Margolis, S.V., Claeys, P., Alvarez, W., Renne, P., Cedillo-Pardoa, E., Maurrasse, F.J.M.R., Curtis, G.H., Smit, J., McWilliams, M.O., 1992. Coeval Ar-40/Ar-39 ages of 65.0 million years ago from Chicxulub crater melt rock and Cretaceous–Tertiary boundary tektites. Science 257, 954–958.

Wignall, P.B., 2001. Large igneous provinces and mass extinctions. Earth-Sci. Rev. 53, 1–33.

Wignall, P.B., Twitchett, R.J., 1996. Oceanic anoxia and the end Permian mass extinction. Science 272, 1155–1158.

Wolbach, W.S., Gilmour, I., Anders, E., Orth, C.J., Brooks, R.R., 1988. Global fire at the Cretaceous–Tertiary boundary. Nature 334, 665–669.

Xu, D.-Y., Ma, S.-L., Chai, Z.-F., Mao, X.-Y., Sun, Y.Y., Zhang, Q.-W., Yang, Z.-Z., 1985. Abundance variation of iridium and trace elements at the Permian/Triassic boundary at Shangsi in China. Nature 314, 154–156.

Yin, H.F., Sweet, W.C., Glenister, B.F., Kotlyar, G., Kozur, H., Newell, N.D., Sheng, J., Yang, Z., Zakharov, Y.D., 1996. Recommendation of the Meishan section as Global Stratotype Section and Point for basal boundary of Triassic System. Newsl. Stratigr. 34, 81–108.

Yin, H., Zhang, K., Tong, J., Yang, Z., Wu, S., 2001. The global stratotype section and point (GSSP) of the Permian–Triassic boundary. Episodes 24, 102–114.

Zhou, L., Kyte, F.T., 1988. The Permian–Triassic boundary event: a geochemical study of three Chinese sections. Earth Planet. Sci. Lett. 90, 411–421.

Zhou, M.F., Zhao, J.H., Qi, L., Su, W.C., Hu, R.Z., 2006. Zircon U–Pb geochronology and elemental and Sr–Nd isotope geochemistry of Permian mafic rocks in the Funing area, SW China. Contrib. Mineral. Petrol. 151, 1–19.